FARL-11 (STRIP1/2) is required for sarcomere and sarcoplasmic reticulum organization in *C. elegans*

Sterling C. T. Martin[a], Hiroshi Qadota[b], Andres F. Oberhauser[c], Jeff Hardin[a,d], and Guy M. Benian[b,*]

[a]Biophysics Program, University of Wisconsin-Madison, Madison, WI 53706; [b]Department of Pathology, Emory University, Atlanta, GA 30322; [c]Department of Neurobiology, The University of Texas Medical Branch, Galveston, TX 77555; [d]Department of Integrative Biology, University of Wisconsin-Madison, Madison, WI 53706

ABSTRACT Protein phosphatase 2A (PP2A) functions in a variety of cellular contexts. PP2A can assemble into four different complexes based on the inclusion of different regulatory or targeting subunits. The B‴ regulatory subunit "striatin" forms the STRIPAK complex consisting of striatin, a catalytic subunit (PP2AC), striatin-interacting protein 1 (STRIP1), and MOB family member 4 (MOB4). In yeast and *Caenorhabditis elegans*, STRIP1 is required for formation of the endoplasmic reticulum (ER). Because the sarcoplasmic reticulum (SR) is the highly organized muscle-specific version of ER, we sought to determine the function of the STRIPAK complex in muscle using *C. elegans*. CASH-1 (striatin) and FARL-11 (STRIP1/2) form a complex in vivo, and each protein is localized to SR. Missense mutations and single amino acid losses in *farl-11* and *cash-1* each result in similar sarcomere disorganization. A missense mutation in *farl-11* shows no detectable FARL-11 protein by immunoblot, disruption of SR organization around M-lines, and altered levels of the SR Ca^{+2} release channel UNC-68.

Monitoring Editor
Ahna Skop
University of Wisconsin, Madison

Received: Mar 8, 2023
Revised: May 16, 2023
Accepted: Jun 6, 2023

INTRODUCTION

A major serine–threonine protein phosphatase that is conserved from yeast to humans is protein phosphatase 2A (PP2A; Shi, 2009). PP2A functions in a wide variety of cellular contexts and forms multiple specific protein complexes via different regulatory or targeting subunits. The PP2A core enzyme comprises a catalytic subunit C (PP2AC) and a scaffolding subunit A (PP2AA). This core forms a complex with a variety of regulatory B subunits, with the B subunits mediating subcellular localization and/or substrate recognition. There are four families of regulatory B subunits: B (B55 or PPP2R2), B′ (B56 or PPP2R5), B″ (B72 or PPP2R3), and B‴ (striatins).

The striatin-interacting phosphatase and kinase (STRIPAK) complex is a PP2A complex in which the regulatory subunit is the protein striatin. Recently, the structure of the STRIPAK complex was solved at 3.2 Å resolution using cryo-EM (Jeong *et al.*, 2021). The complex consists of a catalytic subunit (PP2AC), a scaffolding subunit (PP2AA) called "striatin," striatin-interacting protein 1 (STRIP1), and MOB family member 4 (MOB4). The striatin coiled-coil domain forms an elongated scaffold that links the complex together.

In the budding yeast, *Saccharomyces cerevisiae*, the "Far" complex, originally identified as crucial for pheromone-induced cell cycle arrest, is the yeast counterpart of the STRIPAK complex. The Far complex localizes to the endoplasmic reticulum (ER), and it has been shown that the six Far subunits (Far3, 7, 8, 9, 10, and 11) assemble at the ER in a specific sequence (Pracheil and Liu, 2013): Far9 and Far10 first attach to the ER membrane via their tail-anchor domains; Far3, Far7, and Far8 form a subcomplex that is recruited to the ER by Far9/10; and finally, Far11 binds to the Far3/7/8 subcomplex. Similarly, in *Caenorhabditis elegans*, the nematode orthologue of yeast Far11, called "FARL-11," is localized to the ER and outer nuclear membrane of early embryos and the germ line

This article was published online ahead of print in MBoC in Press (http://www.molbiolcell.org/cgi/doi/10.1091/mbc.E23-03-0083) on June 14, 2023.

Author contributions: S.C.T.M. and H.Q. designed, carried out, and interpreted most of the experiments and wrote some sections of the manuscript; A.F.O. created the protein homology models and interpreted the mutations; J.H. and G.M.B. conceived of the project, provided funding, and edited the manuscript; and G.M.B. carried out a few experiments and wrote most of the paper.

*Address correspondence to: Guy M. Benian (pathgb@emory.edu).

Abbreviations used: ECL, enhanced chemiluminescence; ECM, extracellular matrix; ER, endoplasmic reticulum; HRP, horseradish peroxidase; MHC A, myosin heavy chain A; MMP, Million Mutation Project; mNG, mNeonGreen; PP2A, protein phosphatase 2A; RFP, red fluorescent protein; SIM, structured illumination microscopy; SR, sarcoplasmic reticulum; STRIP1, striatin-interacting protein 1; STRIPAK, striatin-interacting phosphatase and kinase complex.

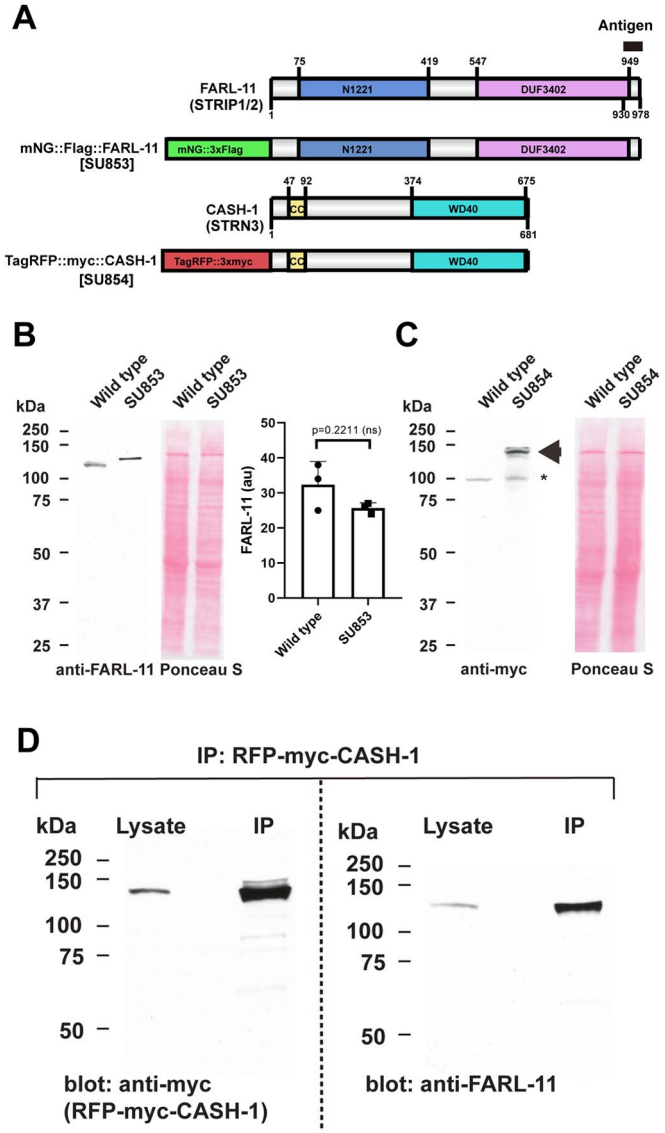

FIGURE 1: Domain organization, tagging design, detection of expression of FARL-11 and CASH-1, and coIP of FARL-11 with CASH-1. (A) Domain organization of FARL-11 and CASH-1 and location of tags. CRISPR/Cas9 was used to create nematode strain SU853, in which consecutive mNeonGreen and Flag tags were added to the N-terminus of FARL-11, and strain SU854, in which RFP and myc tags were added to the N-terminus of CASH-1. "Antigen" refers to the 50 amino acid peptide that was used to generate rabbit antibodies to FARL-11. (B) Western blot demonstrating detection of FARL-11 and mNG-Flag-FARL-11. Nematode extracts were run on a gel, transferred to membrane, and reacted against antibodies to FARL-11. The protein bands detected using anti-FARL-11 ran at sizes expected for endogenous and tagged FARL-11. Western blot reaction on the left, Ponceau staining of the membrane on the right. The graph indicates that the presence of the tag does not significantly affect the level of FARL-11. For each strain, $N = 3$, and significance was tested by a one-tailed students *t* test. (C) Western blot demonstrating detection of RFP-myc-CASH-1 from strain SU854 of expected size (arrow) using antibodies to myc. An additional band of ~100 kDa (asterisk) is detected, but this is also detected in an extract from wild type (no myc tagged proteins expressed), suggesting cross-reactivity of anti-myc to a nematode or bacterial protein. (D) Coimmunoprecipitation of FARL-11 with CASH-1. As described in materials and methods, TagRFP-myc-CASH-1 was immunoprecipitated from a lysate of strain SU854, using nanobodies to RFP coupled to magnetic beads. The left half is a Western blot reacted against antibodies to myc showing that that RFP-myc-CASH-1 was immunoprecipitated from a total protein lysate. On the right is a Western blot reacted against antibodies to FARL-11 indicating that the immunoprecipitate also contains FARL-11. For parts (B), (C), and (D), the positions of molecular weight size markers are indicated.

(Maheshwari *et al.*, 2016). Moreover, in a *farl-11* loss-of-function mutant, the morphology of the ER is severely disrupted, indicating that FARL-11 protein is required for normal ER morphology. In striated muscle, the sarcoplasmic reticulum (SR) is a highly organized, muscle-specific version of the ER and is the storage and release depot for Ca^{2+}. In response to an action potential from motor neurons, the calcium release channel of the SR (the ryanodine receptor) is activated and opens to allow flow of Ca^{2+} from the SR into the muscle cell cytoplasm where Ca^{2+} interacts with components of the sarcomere (usually the troponin/tropomyosin complex) to activate muscle contraction.

The role of STRIPAK in SR function has not been determined. We turned to *C. elegans* as a genetically tractable model organism in which to investigate the function of STRIPAK in muscle function. *C. elegans* is an outstanding system for discovering new conserved aspects of muscle assembly, maintenance, and regulation (Gieseler *et al.*, 2017). In a previous study, we reported that loss of function of most single components of PP2A results in sarcomere disorganization (Qadota *et al.*, 2018). This includes the catalytic subunit C (LET-92), the scaffolding subunit A (PAA-1), regulatory subunit B (SUR-6), regulatory subunit B′ (either PPTR-1 or PPTR-2), regulatory subunit B″ (RSA-1), and regulatory subunit B‴ (CASH-1). Moreover, we reported that with available antibodies to five of these PP2A components, we were able to localize the components to different and overlapping components of the sarcomere. For example, SUR-6 and PPTR-1 localize to I-bands, PPTR-2 localizes to M-lines and dense bodies (Z-disks), and RSA-1 localizes to M-lines and I-bands (Qadota *et al.*, 2018).

Here, we used CRISPR-tagging, antibodies and genetic mutants to investigate the role of the STRIPAK complex in adult *C. elegans* muscle. We report that FARL-11 (STRIP1/2) and CASH-1 (STRN3) are localized to the SR, and that the phenotypes of *farl-11* and *cash-1* loss-of-function mutants are similar. Each mutant shows substantial defects in sarcomere organization, and at least a *farl-11* mutant disrupts SR organization, especially around M-lines.

RESULTS

Mutations in CASH-1 (STRN3) and FARL-11 (STRIP1/2) cause sarcomeric organizational defects

To facilitate our studies, we generated antibodies to a C-terminal portion of FARL-11 and used CRISPR/Cas9 to generate an N-terminal fusion of FARL-11 to mNeonGreen (mNG) and Flag (strain SU853), and an N-terminal fusion of CASH-1 to TagRFP and myc (strain SU854; Figure 1A). As shown in Figure 1B, anti-FARL-11 rabbit polyclonal antibodies react to a protein of the expected size (~120 kDa) from wild type, and an appropriately larger fusion protein from the mNG-tagged strain SU853. As indicated in the graph to the right of Figure 1B, the mNG::3xFlag tagging does not significantly affect the level of expression of FARL-11. Antibodies to myc detect an appropriately sized protein (~140 kDa) from the strain SU854 that expresses an RFP- and myc-tagged fusion to CASH-1 (Figure 1C). An additional band of approximately 100 kDa (indicated by an asterisk in Figure 1C) also reacts to myc antibodies, but this band also appears in an extract from wild type and is thus likely

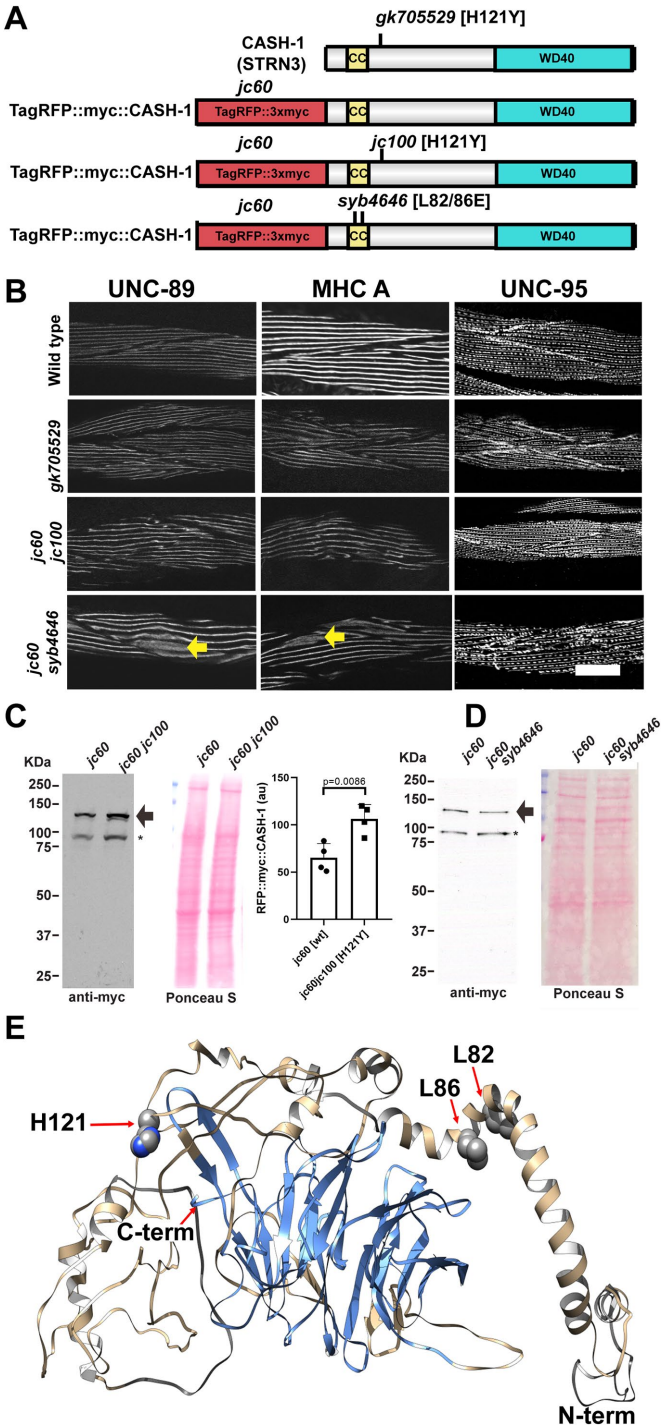

FIGURE 2: Missense mutations in *cash-1* result in mild to moderate disorganization of muscle sarcomeres. (A) Schematic representation of domains in CASH-1 and tagged CASH-1. The H121Y mutation was originally found in the MMP allele *cash-1(gk705529)* and recreated by CRISPR/Cas9 in the RFP-myc tagged *cash-1* strain *jc60*, as *jc60 jc100*. The double missense mutant L82E/L86E was also created by CRISPR/Cas9 in the RFP-myc tagged *cash-1* strain *jc60*, as *syb4646*. (B) Representative images of several body wall muscle cells from wild type, *cash-1(gk705529)*, *cash-1(jc60 jc100)*, and *cash-1(jc60 syb4646)*, immunostained with antibodies to UNC-89 for M-lines, MHC A myosin for A-bands, and UNC-95 for bases of M-lines, dense bodies, and muscle cell boundaries. Mild disorganization of these structures is seen in both strains containing the H121Y missense mutation, with the more severe effect seen with UNC-95 staining, especially at the muscle cell boundaries. A more severe effect on sarcomere and IAC organization is seen in the L82E/L86E double mutant. Yellow arrows point out widening of the localization of UNC-89 and MHC A. Scale bar, 10 µm. (C) and (D) Western blot analysis of the level of RFP-myc-CASH-1 in *cash-1(jc60)* and *cash-1(jc60 jc100)* in C, and *cash-1(jc60 syb4646)* in D. For each, on the left, reaction with anti-myc; on the right, the Ponceau S staining of the blot. Arrows indicate the band expected from RFP-myc-CASH-1; asterisk denotes a cross-reacting band. The presence of the H121Y mutation or the L82E/L86E double mutations does not decrease the level of RFP-myc-CASH-1. As indicated from the graph to the right of part C, the H121Y mutation may increase the level of RFP-myc-CASH-1. For each strain $N = 4$, and significance was tested using a one-tailed Student's *t* test. (E) Structure of CASH-1 based on the human striatin 3 three-dimensional structure (PDB: 7K36) (Jeong *et al.*, 2021) modeled with SWISS-MODEL (Waterhouse *et al.*, 2018) and showing residues L82, L86, and H121. The colors represent different putative WD40 repeats (in blue) and disordered region (in gray).

to represent cross-reactivity to another nematode protein or even a bacterial protein. To seek further evidence of the evolutionary conservation of the STRIPAK complex, we asked whether an in vivo complex could be detected in nematodes that contains both CASH-1 (STRN3) and FARL-11 (STRIP1/2). As shown in Figure 1D, and detailed in Supplemental Figure 1, immunoprecipitation of TagRFP-myc-CASH-1 from an extract of strain SU854, coimmunoprecipitates FARL-11.

In our previous report of the PP2A complex in *C. elegans* muscle, we showed that RNAi knockdown of CASH-1 (STRN3) resulted in adults that are slow-moving and sterile, and by immunostaining with antibodies to myosin, these animals have disorganized sarcomeric A-bands (Qadota *et al.*, 2018). Inspection of the Million Mutation Project (MMP) collection of mutant strains (Thompson *et al.*, 2013) revealed several strains that have missense mutations in conserved residues of CASH-1, but one of them, *cash-1(gk705529)*, which results in a H121Y mutation, had severe phenotypes: a high percentage of embryonic lethality, and, among the animals that reached adulthood, greatly reduced motility. To avoid the confounding influence of the many background mutations in an MMP strain, we recreated the H121Y mutation by CRISPR in our RFP- and myc-tagged CASH-1 strain (*jc100*; Figure 2A). The crystal structure of human striatin 3 coiled-coil domain revealed that it forms a parallel dimer and that two highly conserved residues, L121 and L125, are critical for homodimerization and binding to the A subunit of PP2A (Chen *et al.*, 2014). We used CRISPR to mutate the equivalent leucines (L82 and L86) to glutamates in our RFP- and myc-tagged CASH-1 strain (*syb4646*; Figure 2A). Strains containing the H121Y mutation were adult viable and fertile. However, nematodes homozygous for the L82E/L86E mutations reached adulthood but were sterile, and thus we maintained the mutant chromosome over a balancer chromosome. We immunostained adults from each strain with antibodies to UNC-89 (obscurin) to assess M-lines, myosin heavy chain A (MHC A) to assess A-bands, and UNC-95 to assess the bases of the M-lines and dense bodies (Z-disks) and muscle cell boundaries. As shown in Figure 2B, each of the mutants displays disorganization of these structures, with a more severe phenotype in the L82E/L86E mutant strain. It is interesting that for the L82E/L86E strain, some regions of muscle cells show unusually broad localization of MHC A and especially UNC-89 (indicated by arrows). In addition, UNC-95 staining is moderately disorganized in each mutant strain, especially with respect to the dense bodies and muscle cell boundaries. To assess to what extent the sarcomeric defects could be attributed to

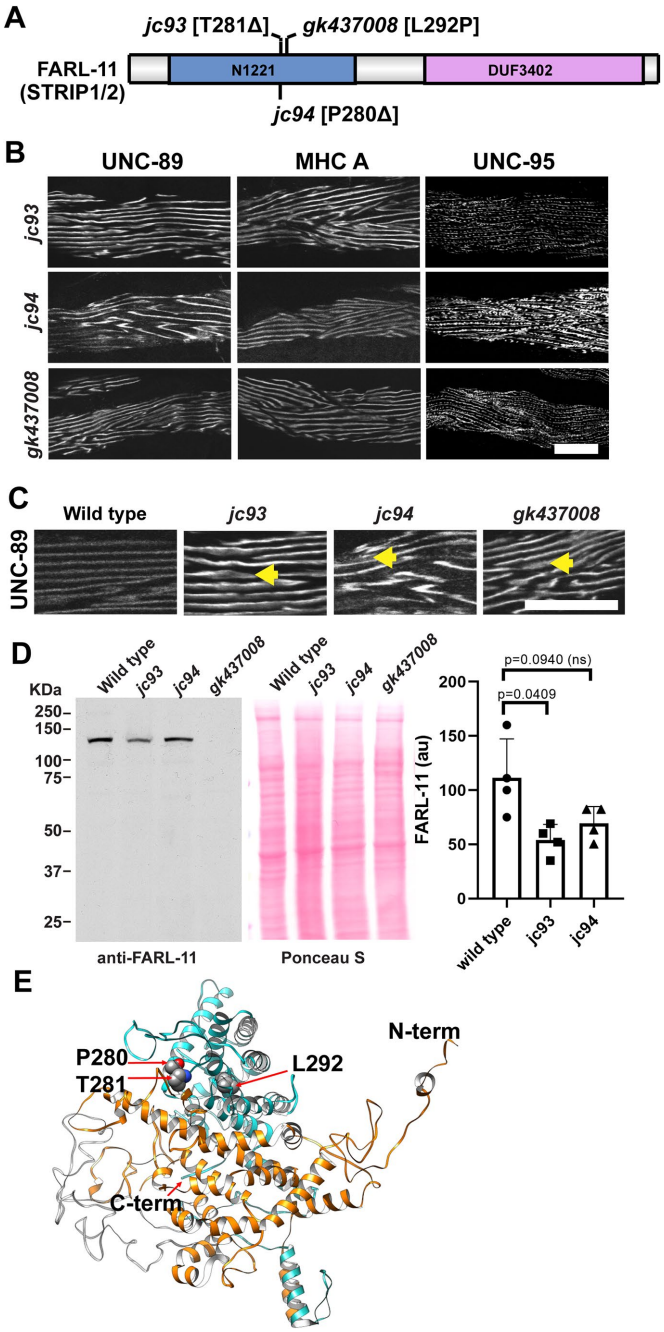

FIGURE 3: Missense mutations in *farl-11* result in disorganization of sarcomeres. (A) Schematic representation of domain organization of FARL-11 and location of mutations. (B) Representative images of several body wall muscle cells from each of *farl-11(jc93)*, *farl-11(jc94)*, and *farl-11(gk437008)*, immunostained with antibodies to UNC-89 for M-lines, MHC A myosin for A-bands, and UNC-95 for bases of M-lines, dense bodies, and muscle cell boundaries. As compared with wild type (top row, Figure 2B), organization of all of these structures is affected. Scale bar, 10 μm. (C) 2× zoomed-in views of immunostaining with anti-UNC-89 showing the moderate to severe mislocalization of UNC-89 in all three mutants compared with wild type. Arrows indicate examples of abnormal broadening of localization. (D) Western blot analysis of the level of FARL-11 in wild type as compared with *farl-11* mutants. On the left, reaction with anti-FARL-11; on the right, the Ponceau S staining of the blot. The L292P substitution in *gk437008* results in no detectable mutant FARL-11 protein. The graph on the right indicates that deletion of single amino acids in mutants *jc93* and *jc94* results in decreased levels of the mutant FARL-11 protein (although for *jc94* not reaching statistical significance). For each strain $N = 4$, and significance was tested using a one-tailed students *t* test. (E) Structure of FARL-11 based on the human STRIP1 three-dimensional structure (PDB: 7K36) (Jeong *et al.*, 2021) modeled with SWISS-MODEL (Waterhouse *et al.*, 2018) and showing residues T281, P280, and L292. The colors represent different putative domains (N1221 in cyan and DUF3402 in orange) and disordered region (in gray).

a decreased level of mutant protein versus functionally defective proteins, we compared the level of the RFP-myc-CASH-1 in an otherwise wild-type background with the level of RFP-myc-CASH-1 H121Y, and RFP/myc-CASH-1 L82E/L86E. As shown in Figure 2C and D, the levels of RFP/myc-CASH-1 were similar in wild type as compared with either H121Y or L82E/L86E mutants. In fact, as indicated in the graph on the right side of Figure 2C, the level of RFP-myc-CASH-1 is increased in the H121Y mutant compared with wild type. Thus, in these missense mutants, the sarcomeric disorganization is most likely due to decreased function rather than decreased levels of the mutant CASH-1 proteins.

To obtain further insight into how these missense mutations affect the function of the CASH-1 protein, we generated a homology model of CASH-1 based on the cryoEM structure of the orthologous human protein, STRN3 (Jeong *et al.*, 2021). Figure 2E displays the locations of the affected residues on this homology model. To predict the potential effects of the mutations, we used the rotamer/mutation tool in Chimera (Pettersen *et al.*, 2004) and then energy minimized to visualize interatomic clashes and contacts based on van der Waals radii. In addition, we used the DynaMut2 (Rodrigues *et al.*, 2021) to predict the effects of the point mutations on protein stability and dynamics. L82 and L86 lie along the surface of a long α-helix (as expected), and we predict that the L82E and L86E mutations will have no significant effect on structure. Nevertheless, as shown for the STRN3, these mutations are likely to affect homodimerization. H121 resides in a loop connecting two α-helices. Given that H121 lies on the surface of the protein, the H121Y could conceivably affect binding to FARL-11.

We selected one *farl-11* MMP allele for analysis, *farl-11(gk437008)*, which has a nonconservative L292 to P change in the N1221 domain (Figure 3A). This strain was outcrossed 3× to wild type. Although we could not create this mutation using CRISPR, we did generate two additional mutations from the CRISPR procedure at nearby residues in this same domain (Figure 3A): *farl-11(jc93)*, which deletes the single amino acid T281 in-frame, and *farl-11(jc94)*, which deletes the single amino acid P280 in-frame. After outcrossing 2× to wild type and immunostaining, all three mutant alleles show severely disorganized sarcomeres (Figure 3B). Of particular note is the wider distribution of both UNC-89 and myosin, similar to what we observed in the *cash-1* mutant containing the L82E/L86E mutations. For the *farl-11* mutants, this wider distribution of UNC-89 and MHC A can be discerned more clearly in the zoomed insets (Figure 3C). To assess to what extent the sarcomeric defect is due to a decreased level of mutant protein versus a functionally defective mutant protein, we compared the levels of FARL-11 protein from all three *farl-11* mutants with wild type. As shown in Figure 3D, Western blot analysis indicates no detectable FARL-11 protein in *farl-11(gk437008)* (L292P). Moreover, both *jc93* and *jc94* show decreased levels of FARL-11, as indicated in the graph in Figure 1D: *jc93* has 48.9% of the wild-type level, and *jc94* has 64.1% of the wild-type level (means, $n = 4$). We were somewhat surprised that

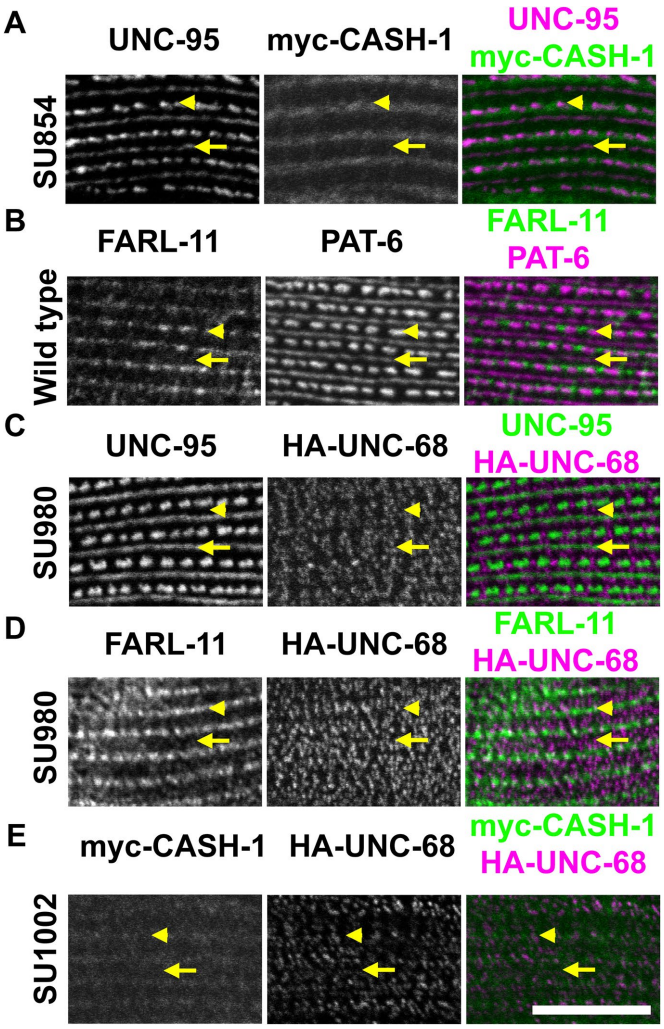

FIGURE 4: Localization of CASH-1, FARL-11, and UNC-68 by confocal microscopy. Each panel shows a portion of a single body wall muscle cell immunostained with antibodies to the indicated proteins or to the myc or HA tags. Yellow arrowheads point to a row of dense bodies; yellow arrows to single M-lines. (A) Strain SU854 (expresses RFP-myc-CASH-1) showing localization of UNC-95 and myc-CASH-1. Myc-CASH-1 localizes between and surrounding dense bodies. (B) Wild type showing localization of PAT-6 and FARL-11. FARL-11 also localizes between and surrounding dense bodies. (C) Strain SU980 (expresses HA-UNC-68) showing localization of UNC-95 and HA-UNC-68. HA-UNC-68 localizes to puncta organized in a striated pattern roughly surrounding dense bodies and M-lines. (D) Strain SU980 showing localization of FARL-11 and HA-UNC-68. The two proteins show partial colocalization suggested by the white puncta created by overlap of green FARL-11 and magenta HA-UNC-68. (E) Strain SU1002 (expresses myc-CASH-1 and HA-UNC-68) showing localization of myc-CASH-1 and HA-UNC-68. The two proteins partially colocalize. Scale bar, 10 μm.

gk437008, a missense mutant, shows no detectable FARL-11 protein. There are no other mutations in the *farl-11* gene in this strain (VC30204), based on a query of the MMP website at Simon Fraser University (http://genome.sfu.ca/mmp/). It should be noted that the penetrance of muscle sarcomeric defects in *cash-1* and *farl-11* mutants is quite high. As indicated in Supplemental Table 1, assessment of 10 adult animals from three mutant alleles of each gene, the penetrance ranges from 70% to 100%, although this varies according to which sarcomeric structure is assessed and according to the presumed strength of mutant alleles. Also, it should be noted that both the penetrance and the severity of phenotype are lower for *cash-1* than for *farl-11*.

To obtain additional understanding about how these mutations might affect the function of FARL-11, we generated an homology model of FARL-11 based on the cryoEM structure of the human orthologue, STRIP1 (Jeong *et al.*, 2021). Figure 3E depicts the locations of the affected residues in this structure. P280 and T281 are located in a highly disordered 47 amino acid loop, and L292 is located in the center of an α-helix. Like for CASH-1, we used the rotamer/mutation tool in Chimera (Pettersen *et al.*, 2004) and the DynaMut2 web tool (Rodrigues *et al.*, 2021) to predict the impact of the mutations on protein stability.

We predict that deletion of either P280 or T281 will have minimal effect on the structure or stability of the protein. This prediction is consistent with the approximately normal abundance of these mutant proteins lacking either residue observed by Western blot (Figure 3D). In contrast, the L292P mutation leads to several interatomic clashes and hence is likely to break the α-helix and lead to a local and even global change in the structure of the protein and lower its stability ($\Delta\Delta G^{Stability} = -0.72$ kcal/mol). Again, our Western blot result on this L292P mutant is consistent with the prediction in that we cannot detect any FARL-11 L292P protein in worm lysates (Figure 3D).

CASH-1 and FARL-11 localize near dense bodies

We next sought to determine the localization of CASH-1 and FARL-11 in nematode body wall muscle. To localize CASH-1, we utilized our CRISPR strain, SU854, which expresses an RFP-myc-CASH-1 fusion protein. As shown in Figure 4A, in which CASH-1 was detected with antibodies to myc, and M-lines and dense bodies detected with antibodies to UNC-95, CASH-1 is localized between and surrounding dense bodies. To localize FARL-11, we used antibodies to FARL-11. As indicated in Figure 4B, in which we costained with antibodies to PAT-6 (α-parvin), which also localizes to the bases of M-lines and dense bodies, FARL-11 localizes between dense bodies and also surrounds dense bodies but not as broadly as CASH-1. Unfortunately, we were not able to address whether CASH-1 and FARL-11 colocalize, despite several attempts. This is probably because the anti-myc-CASH-1 staining produces a low signal and a high background. We also tried to localize the RFP-myc-CASH-1 fusion using antibodies to RFP, and, unfortunately, trials with three different commercial anti-RFP antibodies did not yield better results than anti-myc.

FARL-11 localizes to the SR

Transmission electron micrographs have revealed that the SR in *C. elegans* body wall muscle is restricted to thin membranous sacs closely adjacent to the dense bodies as well as near the bases of M-lines or the middle of the A-band region (Gieseler *et al.*, 2017). In *C. elegans*, the ryanodine receptor or the calcium release channel of the SR is encoded by a single gene, *unc-68* (Maryon *et al.*, 1996; Sakube *et al.*, 1997). Using confocal microscopy to image localization of antibodies to UNC-68 and various components of the myofilament lattice (MHC A, MHC B, vinculin, α-actinin), Maryon *et al.* (1998) concluded that UNC-68 resides primarily in flattened vesicular sacs adjacent to the outer muscle cell membrane in the A-band region. In contrast, Hamada *et al.* (2002), using antibodies to UNC-68 and either rhodamine–phalloidin or antibodies to the A-band protein paramyosin, concluded that UNC-68 resides in the I-band region. Although these two studies seem to give different localizations for UNC-68, together, the results include both known or suspected

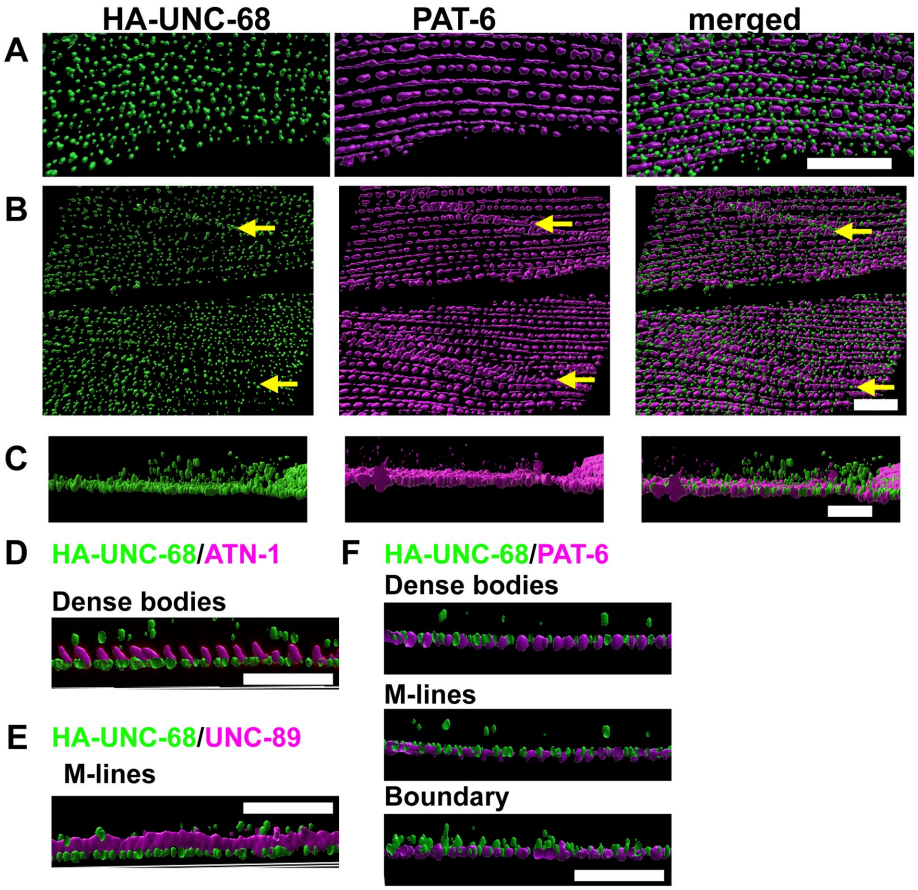

FIGURE 5: Localization of UNC-68 by structured illumination microscopy (SIM). (A–C) Portions of a single or multiple body wall muscle cells from strain SU980 (expresses HA-UNC-68) immunostained with antibodies to PAT-6 and antibodies to HA to visualize HA-UNC-68. PAT-6 is known to localize to the bases of M-lines and dense bodies and to the adhesion plaques of muscle cell boundaries. (A) HA-UNC-68 localizes to puncta situated on either side of M-lines, and surrounding dense bodies, with the largest puncta being closest to the dense bodies. (B) With a wider field of view, HA-UNC-68 can be seen to also localize to muscle cell boundaries, as indicated by arrows. To create images shown in parts C–F, a Z-series of HA-UNC-68 and PAT-6 (or ATN-1 or UNC-89) images from the outer muscle cell membrane to deep into the muscle cell was used to create a three-dimensional reconstruction. (C) Side view of three-dimensional reconstruction of an entire muscle cell showing HA-UNC-68 and PAT-6 localization. For each panel, bottom is close to the outer muscle cell membrane. In addition to being localized like PAT-6 close to the muscle cell membrane, there is substantial localization of HA-UNC-68 in the deeper portions of the muscle cell. (D) Side view of part of a single row of dense bodies costained with HA-UNC-68 and ATN-1. ATN-1 is known to localize to the deepest portions of the dense bodies and defines the deepest portion of the myofilament lattice. HA-UNC-68 is found mainly near the outer muscle cell membrane but also extends deeper into the muscle cell than the myofilament lattice. (E) Side view of part of a single M-line costained with HA-UNC-68 and UNC-89. UNC-89 is known to localize to the entire depth of the M-line and also defines the extent of the myofilament lattice. HA-UNC-68 can be seen localized close to the muscle cell membrane and deeper into the cell than the myofilament lattice. (F) Side view of part of a single row of dense bodies, part of one M-line and part of one muscle cell boundary. Confirming the results in D and E, some HA-UNC-68 is found deeper than the myofilament lattice. In addition, at the muscle cell boundary, HA-UNC-68 is found deeper than PAT-6. Scale bars, 5 μm.

locations of the SR (surrounding dense bodies and adjacent to base of M-lines). Unfortunately, the antibodies generated to UNC-68 utilized in these studies are no longer available. A recent report by Piggott *et al.* (2021) provides the best confocal images of UNC-68 localization in muscle. These authors created a split-GFP knock-in allele for *unc-68* and their confocal images show that GFP::UNC-68 localizes to rows of puncta, some large, some small, but the authors did not colocalize with any sarcomeric markers.

Given that FARL-11 has been localized to the ER of early nematode embryos and that the SR is a muscle-specific type of ER, we used CRISPR/Cas9 to create strain SU980, in which UNC-68 is tagged at its N-terminus with 3xHA. By conventional confocal microscopy, HA-UNC-68 exists in puncta, which are organized in a repeating striated pattern roughly surrounding both dense bodies and M-lines (Figure 4C). We next asked whether FARL-11 and UNC-68 might colocalize. As shown in Figure 4D, there is at least some colocalization of the two proteins, suggested by the white puncta created by the overlap of green FARL-11 and magenta HA-UNC-68 signals. Similarly, HA-UNC-68 and myc-CASH-1 partially colocalize (Figure 4E).

To obtain more information about the localization of UNC-68, we used structured illumination microscopy (SIM), which has an ~120-nm resolution in the XY plane. SIM followed by three-dimensional reconstruction (Figure 5A) shows that HA-UNC-68 localizes to a series of puncta, very similar to the images reported by Piggott *et al.* (2021). Costaining with PAT-6 (α-parvin), which localizes to the bases of the M-lines and dense bodies, reveals that the HA-UNC-68 puncta localize on either side of the M-lines and surround the dense bodies, with the larger puncta being closer to the dense bodies. There is also accumulation of HA-UNC-68 at muscle cell boundaries (indicated by yellow arrows in Figure 5B). When a three-dimensional reconstruction of an entire muscle cell is viewed on its side, we observe that in addition to being localized like PAT-6 close to the muscle cell membrane, there is significant localization of HA-UNC-68 in the deeper portions of the muscle cell (Figure 5C). To determine how deeply this HA-UNC-68 is located, we costained anti-HA with anti-ATN-1 or with anti-UNC-89. ATN-1 localizes to the deepest portions of the dense bodies and defines the deepest portion of the myofilament lattice. As can be seen in Figure 5D, HA-UNC-68 is found mainly near the outer muscle cell membrane but also extends more deeply into the muscle cell than the myofilament lattice. A similar result was observed when HA-UNC-68 was costained with anti-UNC-89 (Figure 5E). To characterize the depth of HA-UNC-68 localization at the muscle cell boundary, we costained HA-UNC-68 and PAT-6. As can be seen at the bottom of Figure 5F, which presents part of one muscle cell boundary, HA-UNC-68 is located more deeply than PAT-6.

Unfortunately, the anti-FARL-11 antibodies did not give a strong enough signal in immunostaining to allow SIM imaging. However, we were able to use confocal microscopy to acquire a Z-series using

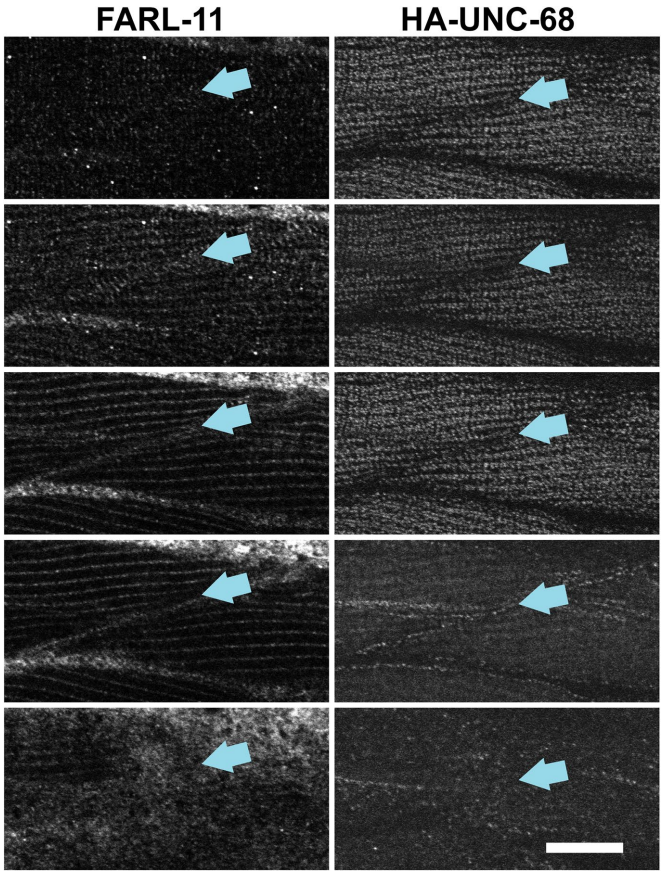

FIGURE 6: A confocal Z-series reveals that FARL-11 localization is similar to localization of HA-UNC-68. Strain SU980 was costained with antibodies to FARL-11 and to HA. From top to bottom are 0.5-µm thick sections from the outer portion of a body wall muscle cell consecutively deeper into the muscle cell. FARL-11 is found between and around dense bodies throughout their depth and is also found at muscle cell boundaries (indicated by the arrows). HA-UNC-68 appears only at the muscle cell boundaries at the deepest portions of the muscle cells (second row from the bottom of the figure). Scale bar, 10 µm.

anti-FARL-11 and anti-SHA for HA-UNC-68, starting from the outer muscle cell membrane to deeper into muscle cells (Figure 6). FARL-11 is found between and around dense bodies throughout their depth and is also found at muscle cell boundaries (indicated by arrows). Curiously, HA-UNC-68 appears only at the muscle cell boundaries at the deepest portions of the muscle cell, again consistent with the SIM images. Localization of UNC-68 at the muscle cell boundaries has not previously been reported and its possible function there is unknown. The function of FARL-11 at muscle cell boundaries, particularly throughout the depth of the boundaries of muscle cells, is also unclear. Overall, FARL-11 localization is similar to that of HA-UNC-68 in Z-series, suggesting that FARL-11 is localized to the SR.

In mammalian muscle, the UNC-89 homologue, obscurin, links myofibrils to the surrounding SR, through interaction of obscurin with the SR membrane proteins small ankyrin 1 and 2 (Bagnato *et al.*, 2003; Kontrogianni-Konstantopoulos *et al.*, 2003). Moreover, knockout of the mouse obscurin gene results in disorganization of the SR (Lange *et al.*, 2009). This role for obscurin/UNC-89 seems to be evolutionarily conserved. In *C. elegans*, there is genetic evidence for an UNC-89 to SR functional linkage. VAV-1 is a RacGEF that regulates the concentration of intracellular calcium and is expressed in body wall muscle; overexpression of *vav-1* in muscle results in slow movement; mutagenesis resulted in suppressors that move better; the suppressor mutations are in *egl-19* (an L-type calcium channel) and *unc-89* (Spooner *et al.*, 2012). Moreover, in *unc-89* mutants, in addition to disorganization of the sarcomeres, there is disorganization of the SR as probed using transgenics overexpressing MYC-UNC-68 or SERCA-GFP (Spooner *et al.*, 2012). Therefore, we wondered whether loss of function of *unc-68*, which has been shown to disrupt SR organization (Maryon *et al.*, 1998), might also disrupt the organization of sarcomeres. As shown in Figure 7, *unc-68(e540)* shows disorganization of major structural components of the sarcomere—the A-bands (MHC A), the M-lines (UNC-89), and the bases of M-lines and dense bodies (UNC-95).

If, as our data suggest, FARL-11 and CASH-1 are components of the SR, one straightforward prediction is that in a mutant in which the SR is disrupted, for example, an *unc-68* mutant, FARL-11 and CASH-1 might be mislocalized. Curiously, however, this is not the case. As shown in Figure 8A, the localization of FARL-11 in *unc-68(e540)* and wild type are nearly identical. Because *cash-1* and *unc-68* are very close together on the genetic map, we used CRISPR to tag CASH-1 at the N terminus using TagRFP::3xmyc in an *unc-68(e540)* mutant background. As shown in Figure 8B, the localization of CASH-1 in *unc-68(e540)* and wild type are nearly identical.

We next tested the hypothesis that FARL-11 and CASH-1 proteins affect the organization of the SR or at least the SR marker UNC-68. To address this, we created two strains, one in which HA-UNC-68 is expressed in *farl-11(gk437008)*, and one in which HA-UNC-68 is expressed in *cash-1(jc100)*. As compared with the localization of HA-UNC-68 in a wild-type background (Figure 9A), the overall density of puncta is reduced, especially near the M-lines, in a *farl-11(gk437008)* mutant background (Figure 9B). However, in a *cash-1(jc100)* mutant background, we observed no change in overall pattern of HA-UNC-68 puncta (Figure 9C). A similar reduction in HA-UNC-68 puncta near the M-lines in *farl-11(gk437008)* was observed when we used the M-line marker UNC-89 (Supplemental Figure 2). To examine this perceived difference quantitatively, we counted the number of puncta around 10 M-lines from each wild type, and *farl-11* and *cash-1* mutants. As shown in Figure 9D, when expressed as the number of puncta per micrometer length of an M-line, *farl-11* shows a substantial decrease compared with wild type (means of 0.75 vs. 1.66 puncta/µm).

Given that the overall density of HA-UNC-68 puncta is reduced in the *farl-11* mutant, we wondered whether there would also be a decrease in the overall level of HA-UNC-68 protein. To address this question, we performed a Western blot in which protein extracts from wild type, *farl-11*(*gk437008*), and *cash-1*(*jc100*) were separated on a 5% polyacrylamide gel. As shown in Figure 10A, anti-HA detects two major protein bands, one running at the expected size of 557–572 kDa (indicated by a blue arrow) and the other running at ~180 kDa (indicated by a yellow arrow). The origin of the ~180 kDa protein is unknown but we suspect that it results from either normal processing of UNC-68 or degradation during extract preparation. The ~180 kDa protein is likely not a nematode or bacterial protein that cross-reacts with antibodies to HA, because it is not detected by Western blot from an extract of wild-type worms (Figure 10B). Quantitation from three experiments shows that, as compared with wild type, 1) the level of the 560 kDa band is not changed in *farl-11* but is increased in *cash-1* (Figure 10C); 2) the level of the 180 kDa band is reduced in both *farl-11* and *cash-1* (Figure 10D); and 3) the combined levels of both the 560 and 180 kDa bands are reduced in

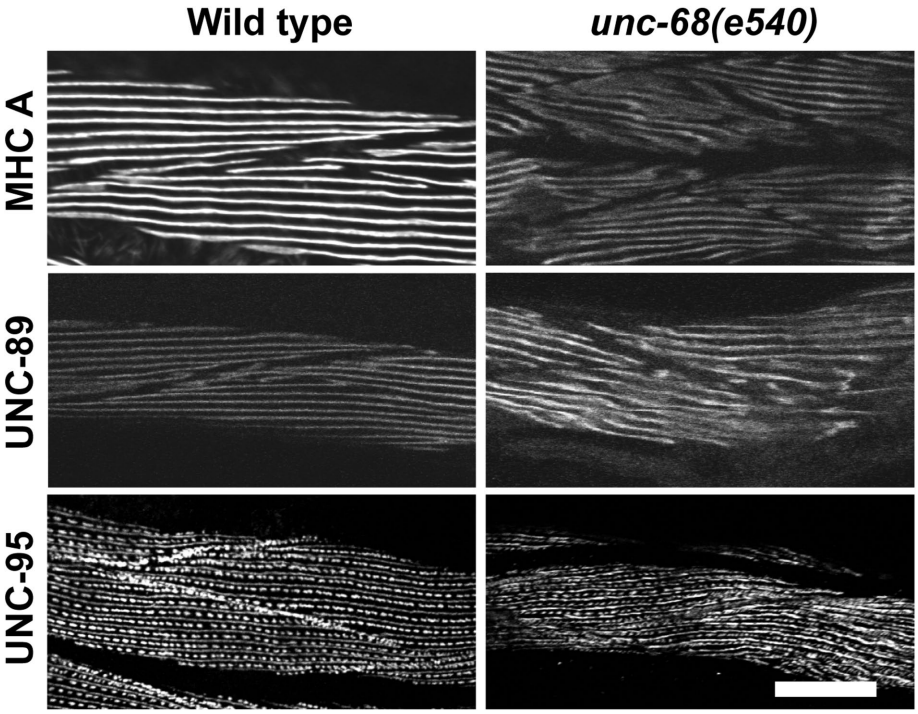

FIGURE 7: Loss of function of *unc-68*, which encodes the SR calcium release channel, results in disorganized sarcomeres. Wild type and mutant *unc-68(e540)* animals were immunostained with antibodies to MHC A myosin, UNC-89, and UNC-95. All the structures labeled by these antibodies (A-bands, M-lines, dense bodies, and muscle cell boundaries) show significant disorganization in *unc-68(e540)*, especially in the organization of UNC-89 and UNC-95. Scale bar, 10 μm.

both *farl-11* and *cash-1* (Figure 10E). Thus, we can conclude that the status of *farl-11* and *cash-1* affects the level of UNC-68, consistent with the reduced number of puncta observed in the *farl-11* mutant.

DISCUSSION

From this study, we have expanded the function of PP2A in striated muscle. We previously reported that loss of function of the catalytic subunit (LET-92) or the scaffolding subunit (PAA-1) results in muscle cells detaching from the extracellular matrix (ECM), and that loss of function of various regulatory (B) subunits results in disorganization of sarcomeres. We had also demonstrated that various components of the PP2A complex localize to various sarcomeric structures (I-band, M-lines, and dense bodies [Z-disks]). We had shown that RNAi for regulatory B''' subunit CASH-1 (STRN3) results in disorganized sarcomeres; however, we did not have reagents available to localize the CASH-1 protein. In the current study, we considered that striatin forms a special PP2A complex, associating not only with catalytic and scaffolding subunits of PP2A but also with STRIP1. The *C. elegans* orthologue of STRIP1 is called "FARL-11," and FARL-11 localizes to the ER and the outer nuclear membrane of early embryos and is required for normal ER organization. This prompted us to determine whether FARL-11 has a role in the muscle-specific ER, the SR. Consistent with the known structure of the human STRIPAK complex, we found that CASH-1 (STRN3) and FARL-11(STRIP1) form a complex in vivo (Figure 1D, Supplemental Figure 1).

Similar to loss of function of canonical PP2A subunits (Qadota *et al.*, 2018), loss of function of CASH-1 (STRN3), or FARL-11 (STRIP1), shows disorganized sarcomeres, including a variable broadening of the distribution of myosin and especially UNC-89 (obscurin) (Figures 2 and 3). We found that both CASH-1 and FARL-11 localize between and surrounding dense bodies (Figures 4 and 11A). We used CRISPR to add an HA tag to the N-terminus of UNC-68 (ryanodine receptor) and localized HA-UNC-68 by SIM to a series of puncta located on either side of the M-lines and surrounding dense bodies, with the larger puncta being closer to the dense bodies (Figures 5, 9, and 11A). Costaining of anti-HA for HA-UNC-68 together with antibodies to FARL-11, or with antibodies to myc for myc-CASH-1, and conventional confocal microscopy, reveals that HA-UNC-68 and myc-CASH-1 partially colocalize (Figure 4, D and E and Figure 6). Unfortunately, neither the anti-FARL-11 antibodies nor the anti-myc antibodies yielded a strong enough signal to allow SIM imaging. However, a Z-series acquired by confocal microscopy after staining with anti-FARL-11 and anti-HA for HA-UNC-68 shows that FARL-11 localization is similar to that of HA-UNC-68 (Figure 6), consistent with FARL-11 being localized to the SR. If CASH-1 and FARL-11 are required for the formation or maintenance of SR, we would expect that disorganization of SR might not affect the localization of CASH-1 or FARL-11, but loss of CASH-1 or FARL-11 might affect the organization of the SR. Our results were consistent with this expectation: an *unc-68* mutant does not affect the localization of FARL-11 or CASH-1 (Figure 8); however, a *farl-11* mutant shows overall reduced density of UNC-68 puncta, especially near the M-lines (Figure 9). Moreover, by Western blot, the overall level of UNC-68 is reduced in both *farl-11* and *cash-1* mutants as compared with wild type (Figure 10).

An interesting effect of mutations in *farl-11* or *cash-1* is a widening of the localization of UNC-89 and MHC A myosin (Figure 2B and Figure 3, B and C). The fact that both UNC-89 and MHC A are affected can be explained by considering that UNC-89 is located throughout the depth of the M-line (Warner *et al.*, 2013), the M-line is the region of the sarcomeric A-band where thick filaments are cross-linked, and MHC A is the myosin isoform that is restricted to the middle of the thick filament in *C. elegans* (Miller *et al.*, 1983). But how loss of function of *farl-11* or *cash-1* results in widening of the M-line region components is more difficult to explain, especially considering that neither FARL-11 nor CASH-1 is localized to the M-line (Figure 11A). One possibility is suggested by our finding that there are reduced numbers of UNC-68-containing puncta around the M-lines (Figure 9). Perhaps the SR sacs that lie on either side of the base of the M-line restrict the growth of the M-line laterally, either by physical hindrance or signaling. In support of this idea, in mammalian striated muscle, obscurin at the M-line links sarcomeres to the surrounding SR by interacting with SR membrane proteins small ankyrins 1 and 2 (Bagnato *et al.*, 2003; Kontrogianni-Konstantopoulos *et al.*, 2003). Another possibility is that with the reduced amount of SR in the *farl-11* mutant, Ca^{+2} signaling is disturbed and this results in unregulated or asymmetric contraction, which ultimately results in disorganization of the sarcomeres. Figure 11 presents a summary of proteins examined in this study and their location in nematode body wall muscle (Figure 11A), and a simple model for results obtained in

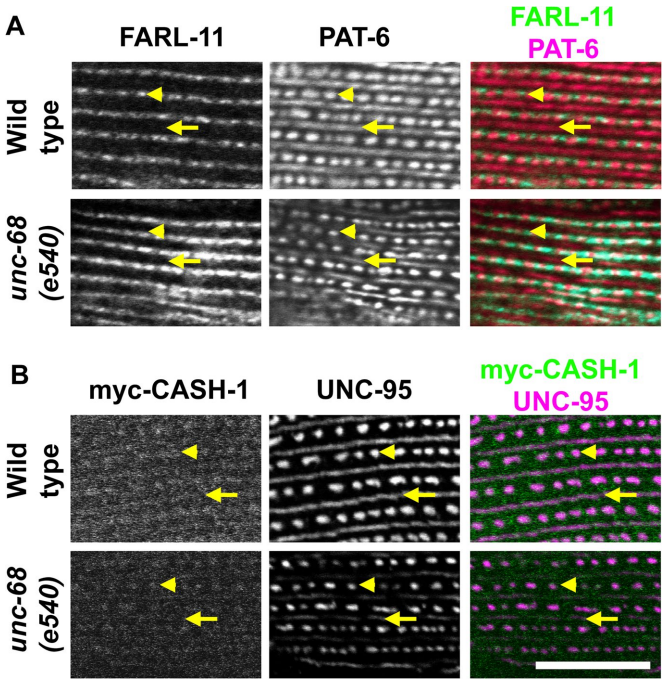

FIGURE 8: Loss of function of *unc-68* does not affect the localization of FARL-11 or CASH-1. (A) Wild type and *unc-68(e540)* were costained with antibodies to FARL-11 and PAT-6. Note that the localization of FARL-11 in *unc-68(e540)* is no different from the localization of FARL-11 in wild type. (B) SU854, which expresses RFP and myc tagged CASH-1, designated "wild type," and SU1086, which expresses RFP and myc tagged CASH-1 and also has the *unc-68(e540)* mutation, designated "*unc-68(e540)*" were costained with antibodies to myc to detect myc-CASH-1 and antibodies to UNC-95 to mark the bases of M-lines and dense bodies. As shown, there is no obvious difference in the localization of myc-CASH-1 in wild type vs. *unc-68(e540)*. Arrowheads point to rows of dense bodies; arrows point to M-lines. Scale bar, 10 µm.

this study (Figure 11B). In this model, the small blue arrow indicates that FARL-11 is important for the normal organization or assembly of the SR (at least near the M-line). The large blue arrow indicates that the SR structure affects sarcomere organization; the orange arrow indicates that alternatively, FARL-11 and CASH-1, are required independently of the SR for sarcomere organization.

We also found that FARL-11 and for the first time that UNC-68 are located at the muscle cell boundaries (Figures 5 and 6), in addition to their locations surrounding M-lines and dense bodies. In addition, a Z-series indicates that UNC-68 appears only at the muscle cell boundaries at the deepest portions of the muscle cell. It should be noted that *C. elegans* spindle-shaped body wall muscle cells are arranged cell to ECM to cell, where attachment plaques of each cell anchor the cell to a thin layer of ECM that lies between the adjacent cells. These attachment plaques are integrin adhesion complexes and contain a subset of proteins found at dense bodies (Qadota *et al.*, 2017). Electron microscopy reveals that the muscle boundaries also contain gap junctions and fingerlike projections of one cell into another cell (Qadota *et al.*, 2017). We had previously speculated that the gap junctions and fingerlike projections provide electrical conductivity, signaling, and structural integrity allowing multiple smaller cells to function as larger units. Although membranous sacs reminiscent of SR have not been found at muscle cell boundaries, perhaps UNC-68 embedded in the cell membranes might facilitate movement of Ca^{+2} between muscle cells.

Finally, we would like to point out that we took advantage of the MMP to identify and study missense mutants in conserved residues in *cash-1* and *farl-11* that developed into adults and were fertile. This allowed us to study adult muscle phenotypes more easily. For example, an intragenic deletion of *farl-11*, *tm6233*, is noted on WormBase to be lethal or sterile.

METHODS

Request a protocol through *Bio-protocol*.

C. elegans strains

N2 (wild type, Bristol)

SU853 *farl-11* (*jc61*[*mNG::TEV::3xflag::farl-11 + LoxP*]) III

SU854 *cash-1* (*jc60*[*TagRFP::TEV::3xmyc::cash-1 +Lox 2272*]) V

SU980 *unc-68*(jc78[*3xha::unc-68*]) V

SU1002 *cash-1* (*jc60*[*TagRFP::TEV::3xmyc::cash-1 +Lox 2272*]; *unc-68*(jc78[*3xha::unc-68*]) V -outcrossed to wild type 2X (o.c. 2x)

SU1047 *farl-11* (*jc93* [*farl-11Δ T281 *jc61*]) II -o.c. 2x

SU1048 *farl-11* (*jc94* [*farl-11 ΔP280 *jc61*]) II

SU1054: *cash-1* (*jc100*[*cash-1 h121y *jc60*]) V-o.c. 2x

SU1086 *cash-1* (*jc106*[*3xmyc::cash-1*]); *unc-68* (*e540*)-o.c. 2x

SU1070 *cash-1* (*jc100*[*cash-1h121y *jc60*]); *unc-68* (*jc78* [*3xha::unc-68*a])-V-o.c. 2x

CB540 *unc-68* (*e540*) V

VC40583 *cash-1* (*gk705529*[*cash-1 H121Y*])-V

VC30204 *farl-11* (*gk437008* [*farl-11 L292P*])-II

GB351 *farl-11*(*gk437008*) [FARL-11 L292P]-II o.c. 3x

GB352 *farl-11*(*gk437008*) [FARL-11 L292P]-II o.c. 3x; *unc-68* (*jc78* [*3xha::unc-68*a])-V

SU1030 cash-1(syb4646[TagRFP::CASH-1 L82E/L86E*jc60])V/tmC12[egl-9(tmIs1197)] V

PHX4646 *cash-1*(*syb4646* [*TagRFP::cash-1 L82E/L86E *jc60*]) V/*nT1* (*qIs51*)] (IV; V)

CRISPR/Cas9

To generate endogenous insertions, a self-excising cassette was used as described (Dickinson *et al.*, 2015). *tagrfp::SEC::CASH-1/+* was crossed into the *tmC12* (Dejima *et al.*, 2018) balancer to facilitate SEC removal. *mng::SEC::farl-11/+* was crossed into the *mIn1* balancer to facilitate SEC removal. The balanced progeny were heat shocked at 34°C to remove the SEC. SEC excision and correct knock-in were confirmed by PCR of nonrolling, nonbalanced progeny. Worms were outcrossed with N2 a minimum of 2x.

SunyBiotech generated the PHX4646 *cash-1*(*syb4646* [*TagRFP::cash-1 L82E/L86E *jc60*])V/*nT1* (*qIs51*)] (IV; V) strain. This strain was outcrossed with N2 and then crossed into the *tmC12* [*egl-9*(*tmIs*1197)] strain to create SU1030 *cash-1* (*syb4646* [*TagRFP::cash-1 L82E/L86E *jc60*])V/*tmC12* [*egl-9*(*tmIs*1197)] V

Single point mutants were generated as described (Arribere *et al.*, 2014).

Guide RNA sequences were cloned into the Cas9 containing plasmid (pJW1219).

CASH-1 TagRFP 5′ guide- 5′ -CGGATTCGAGTAGTTACAATGG
CASH-1 H121Y guide- 5′ ATTTATGTATGCATCAAGGT
CASH-1 L28E/L86E guide 1-GCTCGTATTGCTTTCCTACAAGG
CASH-1 L82E/L86E guide 2-AATTATCGACTAACCCACAACGG

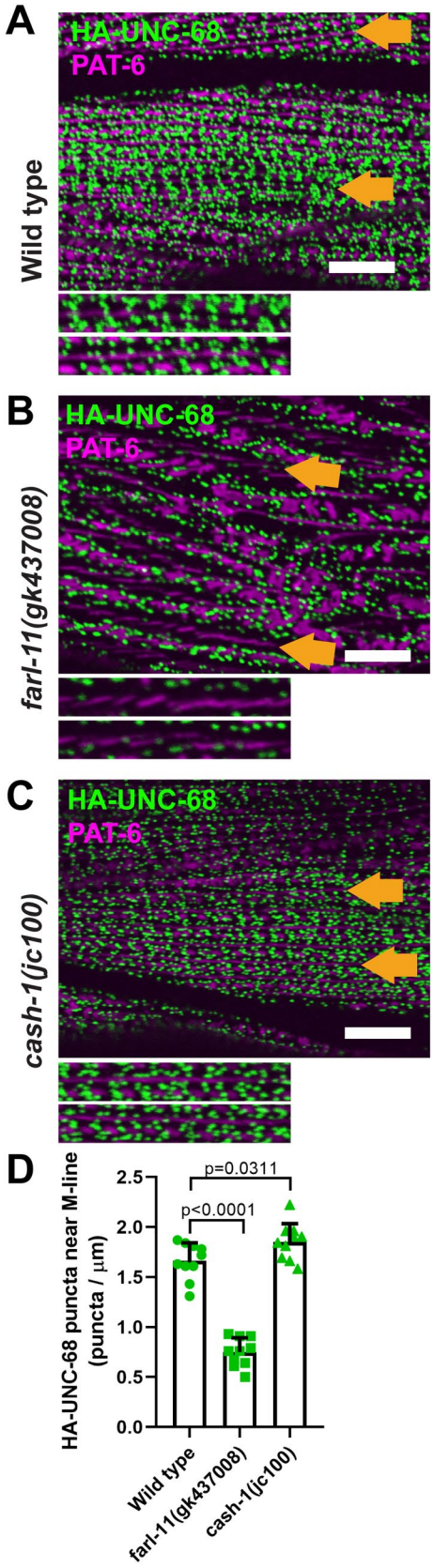

FIGURE 9: The organization of UNC-68 is adversely affected by loss of function of *farl-11*. Confocal imaging of body wall muscle costained with antibodies to HA to detect HA-UNC-68 and antibodies to PAT-6. Scale bar, 10 µm. (A) Imaging of SU980, which expresses HA-UNC-68 in a wild-type background. The two thin rectangles at the bottom are zoomed-in images of the areas denoted by the orange arrows. Note the accumulation of HA-UNC-68 small puncta around M-lines (magenta lines of PAT-6 staining). (B) Imaging of GB352, which expresses HA-UNC-68 in a *farl-11(gk437008)* mutant background. Note that in the zoomed-in images there are fewer HA-UNC-68 small puncta surrounding M-lines, as compared with what is observed in a wild-type background shown in (A). (C) Imaging of SU1070, which expresses HA-UNC-68 in a *cash-1(jc100)* mutant background. Note that in the zoomed-in images UNC-68 small puncta have the same density and arrangement of distribution around M-lines as in the wild-type background shown in (A). (D) Quantitation of HA-UNC-68 puncta near M-lines in wild type and the two mutants. For each strain, 5–6 confocal images were taken and 10 M-lines were chosen randomly. A rectangle was placed around each M-line, with dimensions 600 × 40 pixels (with length ~34.3 µm) and the number of puncta recorded, and this number divided by the length of the rectangle. As indicated on the graph, *farl-11(gk437008)* shows a statistically significant ($p < 0.0001$) reduction in the number of these HA-UNC-68 puncta as compared with wild type.

FARL-11-mNG 5′ guide: - 5′GGCCTGATTCCCATTACATT
FARL-11 L290P guide-5′ ATTTCATTATCAACCATAGT
UNC-68-5′guide-5′ TCCTCCCTGCTCCTCCTTGT

Homology searches/protein sequence analysis

CASH-1 and FARL-11 protein sequences were run through a Hydrophobic Cluster analysis program (mboyle@RPBS) to generate a Hydrophobic Cluster Plot (Néron *et al.*, 2009). *jc93*, *jc94*, and *jc100* were generated at sites of predicted secondary structure (Callebaut *et al.*, 1997). *cash-1 L82E/L86E* mutations were designed to mimic the mutations in the homodimerization domain of STRN-3 (Chen *et al.*, 2014).

Protein structure modeling

For FARL-11 (uniprot Q19300) and CASH-1 (uniprot G5EE12) protein structure modeling, CLUSTALW version 1.2.2 (https://www.ebi.ac.uk/Tools/msa/clustalw2/), SWISS-MODEL version July 2021 (https://swissmodel.expasy.org/; Waterhouse *et al.*, 2018), and Phyre2 version 2.0 (http://www.sbg.bio.ic.ac.uk.phyre2/html/page.cgi?id=index; Kelley *et al.*, 2015) online tools were used.

For FARL-11, we used the cryoEM structure of human orthologue of STRIP1 as reference for modeling (7K36.pdb; Jeong *et al.*, 2021). For CASH-1, we used the human orthologue STRN3 as reference for modeling (7K36.pdb; Jeong *et al.*, 2021). Molecular graphics were generated by using Chimera version 1.15 (https://www.cgl.ucsf.edu/chimera/; Pettersen *et al.*, 2004). Single amino acid mutations were inserted using the rotamer tool and then energy minimized to minimize interatomic clashes and contacts based on van der Waals radii. In addition, we used the DynaMut2 (Rodrigues *et al.*, 2021) to predict the effects of the point mutations on protein stability and dynamics.

FARL-11 antibody production

Antibody production was performed by Li International (Denver, CO). A 50 amino acid chemically synthesized peptide corresponding to the extreme C-terminus of FARL-11 (aa 929-978 TCAHSVLGANLKLGRHFKKDYEKWLEQEVFNASIDWDKLLIETRGVEDLM) was injected into New Zealand rabbits. Li International performed immunization and provided lyophilized antibody, which was resuspended to 1 mg/ml with 1× PBS.

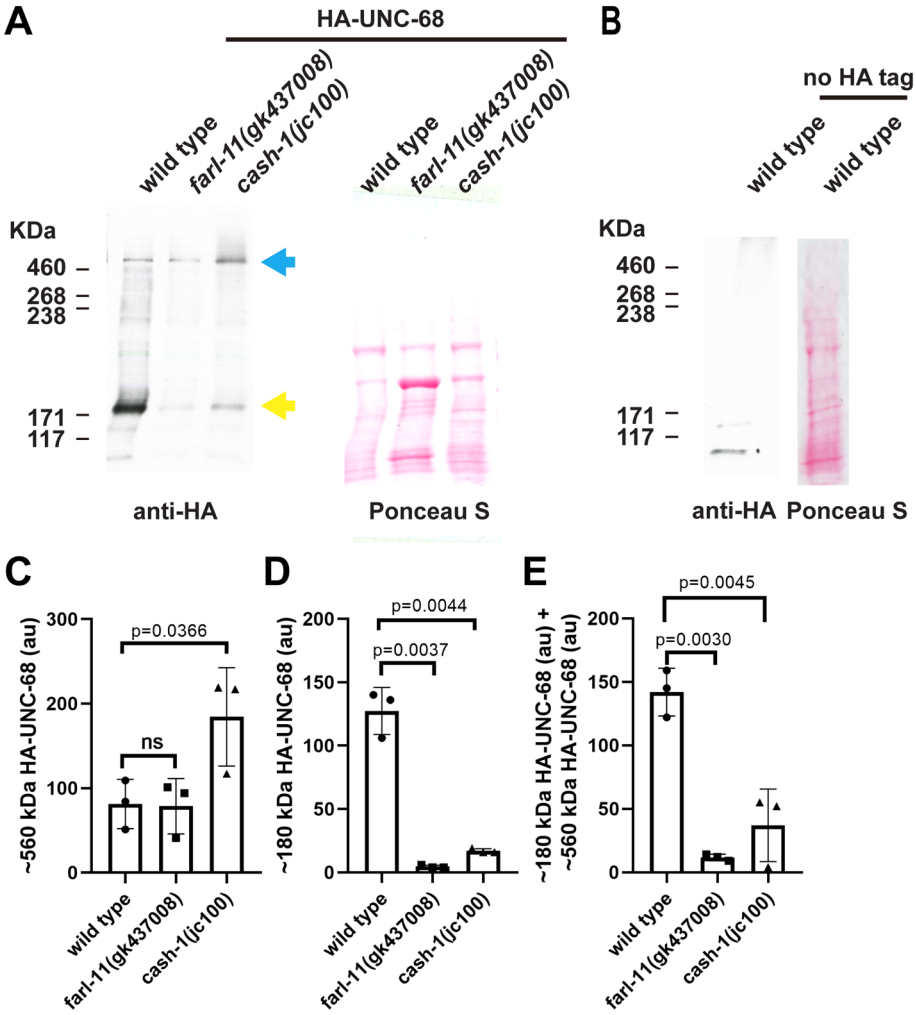

FIGURE 10: The level of HA-UNC-68 and/or its fragments are affected by loss of function of *farl-11* and *cash-1*. (A) Total protein extracts from strains expressing HA-UNC-68 in wild type, *farl-11* and *cash-1* mutant backgrounds were separated on 5% SDS–PAGE, transferred to membrane, and reacted with antibodies to HA. On the left is the western reaction, and on the right is the membrane stained with Ponceau S. Molecular weight size markers are shown on the far left. The blue arrow indicates the position of the full-length HA-UNC-68, which is expected to be 557–572 KDa (multiple isoforms); the yellow arrow points to a likely N-terminal ~180 KDa fragment from HA-UNC-68. (B) A total protein extract from wild type (no HA-tagged proteins expressed) was similarly separated on a 5% gel, blotted, reacted with anti-HA, and exposed to film for the same time as the blot shown in (A). Note that a protein of ~180 kDa is not detected. (C–E) Quantitation of the levels of the 560 kDa, 180 kDa, and the sum of both proteins, comparing wild type with *farl-11* and *cash-1* mutants. For each strain $N = 3$, and significance was tested by a one-tailed Student's *t* test.

Coimmunoprecipitation of FARL-11 with CASH-1

For Supplemental Figure 1, coimmunoprecipitation was performed essentially as described (Zaidel-Bar *et al.*, 2010). Twenty, 10-cm NGM plates with gravid adults were harvested and frozen in Lysis (–) buffer (50-mM HEPES pH 7.4, 150-mM NaCl, 0.05-mM DTT). Worms were lysed by sonication in Lysis (+) buffer (50-mM HEPES pH 7.4, 150-mM NaCl, 0.05-mM DTT, 1% NP-40) and total lysates were centrifuged at 4°C. The supernatant was then precleared using ChromoTek control magnetic agarose beads (ChromoTek, cat. no. gmab-20) for 30 min at 4°C. Precleared lysates were then incubated with ChromoTek RFP-Trap magnetic agarose beads (cat. no. rtma-20) for 1 h at 4°C to bind to TagRFP-myc-CASH-1. Beads were washed 3× with 1 ml of Lysis (–) buffer and eluted with 50 µl of Lysis (–) buffer at 90°C for 10 min. Samples were resolved on 10% SDS–PAGE and transferred to PVDF membrane (Immobilon-FL, Millipore, cat. no. IPFL00010) using a ThermoFisher Powerblotter (cat. no. PB0013), and immunoblotting was performed using ThermoFisher Scientific (Waltham, MA) iBindFlex (cat. no. SLF2000). FARL-11 was detected at 1:500 dilution using the rabbit anti-FARL-11 antibody described above. LiCor 2° goat anti-rabbit antibody (cat. no. 925-3211) was used for detection at 1:4000 dilution.

For Figure 1D, coimmunoprecipitation was performed as follows. A large quantity of worms (~3 ml packed) from strain SU854 was grown on 19, 15-cm high-peptone NGM plates seeded with *E. coli* strain NA22, and a "worm powder" was generated by grinding the worms extensively in a mortar and pestle in liquid nitrogen. A total protein lysate (Lysate) was prepared by adding worm powder to 1 ml of Lysis Buffer (50-mM Tris pH 7.5, 150-mM NaCl, 1% NP40, 0.05-mM DTT, 1-mM EDTA, cOmplete Mini protease inhibitor cocktail [Roche], 1-mM PMSF) at a ratio of approximately 20% volume to volume, vortexing for 1 min, incubating on ice for 2 min, vortexing for 2 min, and then spinning at top speed in a microfuge at 4° for 10 min, and saving the supernatant. A portion was saved and diluted 1:1 with 2X Laemmli loading buffer to run on a gel. To the remainder of the supernatant was added 30 µl of RFP-Trap Magnetic Particles M-270 (cat. no. rtd-20, ChromoTek), incubating on a rotating wheel at 4° for 50 min, removing the beads from the solution using a rack containing neodymium magnets, and then washing the beads with 1-ml Wash Buffer (50-mM Tris pH 7.5, 150-mM NaCl, 0.05-mM DTT, 1-mM EDTA, cOmplete Mini protease inhibitor cocktail (Roche), 1-mM PMSF) 3×. To the washed beads was added 33 µl of 2X Laemmli sample buffer, vortexing for 5 s, heating at 95° for 5 min, vortexing for 5 s, and then separating out the beads on the magnetic stand; the resulting liquid designated as "IP." Multiple lanes containing either 20 µl of Lysate or IP were separated on a 10% SDS–PAGE, transferred to nitrocellulose membrane, and as shown in Figure 1D, one portion reacted against anti-C-Myc (catalogue number M4439, Sigma-Aldrich, St. Louis, MO at 1:3000 dilution), or affinity-purified anti-FARL-11 at 1:1000 dilution, reacted with the appropriate horseradish peroxidase (HRP)-conjugated secondary antibodies, and visualized with enhanced chemiluminescence (ECL) reagents (cat. no. 32106, Thermo Scientific) and exposure to film.

Western blots

The method of Hannak *et al.* (2002) was used to prepare total protein lysates from mixed-stage populations of wild-type, SU853, SU854, SU1054, *farl-11(jc93)*, *farl-11(jc94)*, *farl-11(gk437008)*, SU980, GB352,

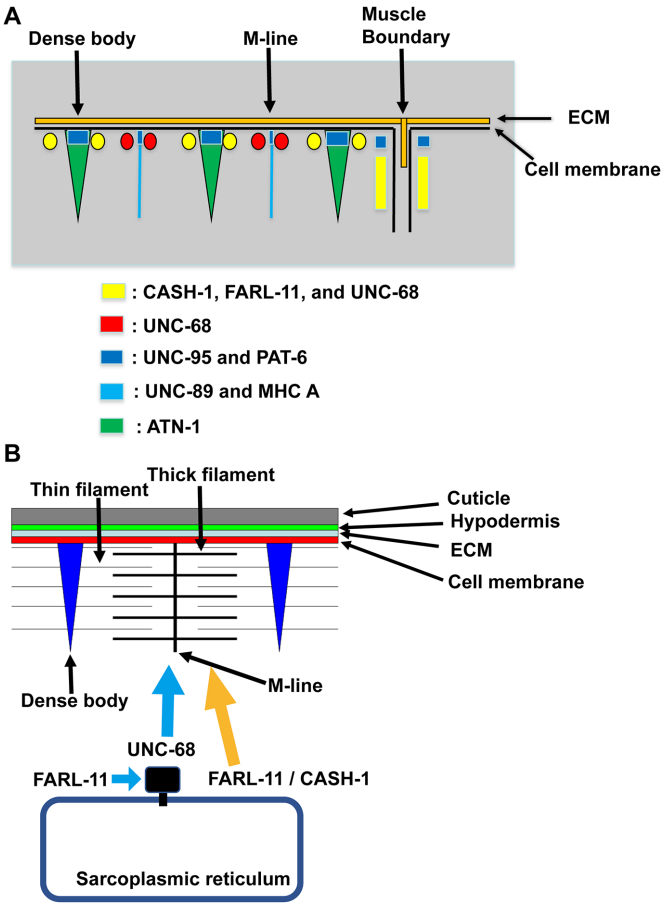

FIGURE 11: Location of proteins and a model for the results obtained from this study. (A) Schematic of a portion of two nematode body wall muscle cells depicting several sarcomeres and the muscle cell boundary. The sarcoplasmic reticulum (SR) is not shown but consists of membranous sacs lying on either side of the M-line close to the muscle cell membrane and closely associated to the sides of the dense bodies (Gieseler *et al.*, 2017). The names of the mammalian orthologues are shown within parentheses: CASH-1 (striatin), FARL-11 (STRIP1/2), UNC-68 (ryanodine receptor), PAT-6 (α-parvin), UNC-89 (obscurin), MHC A (myosin heavy chain), and ATN-1 (α-actinin). UNC-95 and PAT-6 have been previously shown to localize to the bases of dense bodies and M-lines and the muscle cell boundaries. UNC-89 is located throughout the depth of the M-line, MHC A is located in the center of the A-band, and ATN-1 is located in the major and deeper portion of the dense body. In this study, we show that FARL-11 and CASH-1 are likely to reside in the SR near the dense bodies (yellow dots) because of their colocalization with the known SR marker UNC-68. UNC-68 is located surrounding the bases of the dense bodies (yellow dots) and M-lines (red dots). Interestingly, CASH-1, FARL-11, and UNC-68 also reside at the deeper portions of the muscle cell boundaries (yellow rectangles). (B) A model for functional interactions. Because deficiency of FARL-11 results in loss of UNC-68 puncta around M-lines and altered levels of UNC-68 protein, FARL-11 is required for proper SR organization (small blue arrow). Because loss of function of either *farl-11* or *cash-1* results in disorganized sarcomeres, STRIPAK is likely to be required for proper sarcomere organization directly (large orange arrow) and/or indirectly through its altered SR organization or calcium signaling (large blue arrow).

and SU1070 worms. For the Western blots presented in Figures 1–3, equal amounts of total protein were separated on 10% polyacrylamide-SDS-Laemmli gels, transferred to nitrocellulose membranes, reacted with affinity purified, anti-FARL-11 at 1:500 or 1:1000 dilution, and anti-myc (mouse monoclonal clone 9E 10 from the University of Iowa Hybridoma Bank) at 1:300 dilution. Blots were reacted with antirabbit (or antimouse) immunoglobulin G conjugated to HRP (GE HealthCare) at 1:10,000 dilution and visualized by ECL. For the Western blot comparing the level of HA-UNC-68 in wild-type versus *farl-11* and *cash-1* mutant backgrounds shown in Figure 10, equal amounts of total protein from each of these strains were separated by a 5% separating and 3% stacking Laemmli SDS–PAGE gel, transferred to nitrocellulose membrane for 2 h, and reacted with anti-HA (rabbit monoclonal antibody from Cell Signaling Technologies, cat. no. 3724S) at 1:1000 dilution, followed by reaction with antirabbit immunoglobulin G conjugated to HRP (GE HealthCare) at 1:10,000 dilution and visualized by ECL. For protein molecular weight size markers, we used the HiMark Pre-Stained Protein Standard (cat. no. LC5699 from Life Technologies). For comparison of protein levels between wild type and mutants, samples were normalized based on total protein per lane visualized by Ponceau S staining.

Immunostaining, confocal, and SIM microscopy of body wall muscle

Adult nematodes were fixed and immunostained using the method described by Nonet *et al.* (1993) with further details described in Wilson *et al.* (2012). The following primary antibodies were used at 1:200 dilution except as noted: anti-UNC-89 (mouse monoclonal MH42; Hresko *et al.*, 1994; Benian *et al.*, 1996), anti-MHC A (mouse monoclonal 5-6; Miller *et al.*, 1983), anti-UNC-95 (rabbit polyclonal Benian-13; Qadota *et al.*, 2007), anti-PAT-6 (rat polyclonal; Warner *et al.*, 2013), anti-ATN-1 (mouse monoclonal MH35; Francis and Waterston, 1991), anti-HA (rabbit monoclonal from Cell Signaling Technology, cat. no. 3724S; and mouse monoclonal from Sigma-Aldrich, cat. no. H3663), anti-myc (mouse monoclonal clone 9E 10 from the University of Iowa Hybridoma Bank), and anti-FARL-11 (this study). Secondary antibodies, used at 1:200 dilution, included anti-rabbit Alexa 488, antirat Alexa 594, and antimouse Alexa 594, all purchased from Invitrogen. Images were captured at room temperature with a Zeiss confocal system (LSM510) equipped with an Axiovert 100M microscope and an Apochromat x63/1.4 numerical aperture oil immersion objective, in 1× and 2.5× zoom mode. For imaging Alexa 488, the excitation was conducted using a 488-nm Argon laser, and emission was captured using a 505–530 nm bandpass filter. For imaging Alexa 594, the excitation was conducted using a 543-nm Helium–Neon laser, and emission >560 nm was captured using a longpass filter. Super-resolution microscopy was conducted with a Nikon N-SIM system in three-dimensional structured illumination mode on an Eclipse Ti-E microscope equipped with a 100 × /1.49 NA oil immersion objective, 488- and 561-nm solid-state lasers, and an EM-CCD camera (DU-897, Andor Technology). For imaging Alexa 488, we used a 470–490 nm excitation filter and a 500–545 nm emission filter. For imaging Alexa 594, we used a 556- to 566-nm excitation filter and a 570- to 640-nm emission filter. Super-resolution images were reconstructed using the N-SIM module in NIS-Elements software. For all images, confocal and SIM, color balance was adjusted by using Adobe Photoshop (Adobe, San Jose, CA).

ACKNOWLEDGMENTS

H.Q. and G.M.B. were supported by the National Institutes of Health (NIH) grant R01HL160693 and the National Science Foundation (NSF) grant 2050009. J.H. and S.C.T.M. were supported by NIH grants R01GM058038 and MIRA R35GM145312. A.F.O. acknowledges support from The Cecil and Ida Green Endowment. In addition, S.C.T.M. was supported by an NIH T32 (GM130550) Biophysics

Training Grant, a Gilliam Fellowship from the Howard Hughes Medical Institute, an Advanced Opportunities Fellowship, and a COVID-19 dissertation completion fellowship from the University of Wisconsin-Madison.

REFERENCES

Arribere JA, Bell RT, Fu BXH, Artiles KL, Hartman PS, Fire AZ (2014). Efficient marker-free recovery of custom genetic modifications with CRIPSR/Cas9 in Caenorhabditis elegans. Genetics 198, 837–846.

Bagnato P, Barone V, Giacomello E, Rossi D, Sorrentino V (2003). Binding of an ankyrin-1 isoform to obscuring suggests a molecular link between the sarcoplasmic reticulum and myofibrils in striated muscles. J Cell Biol 160, 245–253.

Benian GM, Tinley TL, Tang X, Borodovsky M (1996). The Caenorhabditis elegans gene unc-89, required for muscle M-line assembly, encodes a giant modular protein composed of Ig and signal transduction domains. J Cell Biol 132, 835–848.

Callebaut I, Labesse G, Durand P, Poupon A, Canard L, Chomilier J, Henrissat B, Mornon JP (1997). Deciphering protein sequence information through hydrophobic cluster analysis (HCA): current status and perspectives. Cell Mol Life Sci 53, 621–645.

Chen C, Shi Z, Zhang W, Chen M, He F, Zhang Z, Wang Y, Feng M, Wang W, Zhao Y, *et al*. (2014). Striatins contain a noncanonical coiled coil that binds protein phosphatase 2A A subunit to form a 2:2 heterodimeric core of striatin-interacting phosphatase and kinase (STRIPAK) complex. J Biol Chem 289, 9651–9661.

Dejima K, Hori S, Iwata S, Suehiro Y, Yoshina S, Motohashi T, Mitani S (2018). An aneuploidy-free and structurally defined balancer chromosome toolkit for Caenorhabditis elegans. Cell Rep 22, 232–241.

Dickinson DJ, Pani AM, Heppert JK, Higgins CD, Goldstein B (2015). Streamlined genome engineering with a self-excising drug selection cassette. Genetics 200, 1035–1049.

Francis R, Waterston RH (1991). Muscle cell attachment in *Caenorhabditis elegans*. J Cell Biol 114, 465–479.

Gieseler K, Qadota H, Benian GM (2017). Development, structure and maintenance of *C. elegans* body wall muscle. In: WormBook, ed. The *C. elegans* Research Community, WormBook, doi/10.1895/wormbook.1.81.2; http://www.wormbook.org.

Hamada T, Sakube Y, Ahnn J, Kim DH, Kagawa H (2002). Molecular dissection, tissue localization and Ca2+ binding of the ryanodine receptor of Caenorhabditis elegans. J Mol Biol 324, 123–135.

Hannak E, Oegema K, Kirkham M, Gonczy P, Habermann B, Hyman AA (2002). The kinetically dominant assembly pathway for centrosomal asters in Caenorhabditis elegans is gamma-tubulin dependent. J Cell Biol 157, 591–602.

Hresko MC, Williams BD, Waterston RH (1994). Assembly of body wall muscle and muscle cell attachment structures in Caenorhabditis elegans. J Cell Biol 124, 491–506.

Jeong B-C, Bae SJ, Ni L, Zhang X, Bai X-C, Luo X (2021). Cryo-EM structure of the Hippo signaling integrator human STRIPAK. Nature Struct Mol Biol 28, 290–299.

Kelley LA, Mezulis S, Yates CM, Wass MN, Sternberg MJ (2015). The Phyre2 web portal for protein modeling, prediction and analysis. Nat Protoc 10, 845–858.

Kontrogianni-Konstantopoulos A, Jones EM, Van Rossum DB, Bloch RJ (2003). Obscurin is a ligand for small ankyrin 1 in skeletal muscle. Mol Biol Cell 14, 1138–1148.

Lange S, Ouyang K, Meyer G, Cui L, Cheng H, Lieber RL, Chen J (2009). Obscurin determines the architecture of the longitudinal sarcoplasmic reticulum. J Cell Sci 122, 2640–2650.

Maheshwari R, Pushpa K, Subramaniam K (2016). A role for post-transcriptional control of endoplasmic reticulum dynamics and function in C. elegans germline stem cell maintenance. Development 143, 3097–3108.

Maryon EB, Coronado R, Anderson P (1996). unc-68 encodes a ryanodine receptor involved in regulating C. elegans body-wall muscle contraction. J Cell Biol 134, 885–893.

Maryon EB, Saari B, Anderson P (1998). Muscle-specific functions of ryanodine receptor channels in Caenorhabditis elegans. J Cell Sci 111, 2885–2895.

Miller DM 3rd, Ortiz I, Berliner GC, Epstein HF (1983). Differential localization of two myosins within nematode thick filaments. Cell 34, 477–490.

Néron B, Menager H, Maufrais C, Joly N, Maupetit J, Letort S, Carrere S, Tuffery P, Letondal C (2009). Mobyle: a new full web bioinformatics framework. Bioinformatics 25, 3005–3011.

Nonet ML, Grundahl K, Meyer BJ, Rand JB (1993). Synaptic function is impaired but not eliminated in C. elegans mutants lacking synaptotagmin. Cell 73, 1291–1305.

Pettersen EF, Goddard TD, Huang CC, Couch GS, Greenblatt DM, Meng EC, Ferrin TE (2004). UCSF Chimera—a visualization system for exploratory research and analysis. J Comput Chem 25, 1605–1612.

Piggott CA, Wu Z, Nurrish S, Xu S, Kaplan JM, Chisholm AD, Jin Y (2021). Caenorhabditis elegans junctophilin has tissue-specific functions and regulates neurotransmission with extended-synaptotagmin. Genetics 218, iyab063.

Pracheil T, Liu Z (2013). Tiered assembly of the yeast Far3-7-8-9-10-11 complex at the endoplasmic reticulum. J Biol Chem 288, 16986–16997.

Qadota H, Matsunaga Y, Bagchi P, Lange KI, Carrier KJ, Pols WV, Swartzbaugh E, Wilson KJ, Srayko M, Pallas DC, Benian GM (2018). Protein phosphatase 2A is crucial for sarcomere organization in Caenorhabditis elegans striated muscle. Mol Biol Cell 29, 2084–2097.

Qadota H, Matsunaga Y, Nguyen KCQ, Mattheyses A, Hall DH, Benian GM (2017). High-resolution imaging of muscle attachment structures in Caenorhabditis elegans. Cytoskeleton 74, 426–442.

Qadota H, Mercer KB, Miller RK, Kaibuchi K, Benian GM (2007). Two LIM domain proteins and UNC-96 link UNC-97/pinch to myosin thick filaments in Caenorhabditis elegans muscle. Mol Biol Cell 18, 4317–4326.

Rodrigues CHM, Pires DEV, Ascher DB (2021). DynaMut2: assessing changes in stability and flexibility upon single and multiple point missense mutations. Protein Sci 30, 60–69.

Sakube Y, Ando H, Kagawa H (1997). An abnormal ketamine response in mutants defective in the ryanodine receptor gene ryr-1 (unc-68) of Caenorhabditis elegans. J Mol Biol 267, 849–864.

Shi Y (2009). Serine/threonine phosphatases: mechanism through structure. Cell 139, 468–484.

Spooner PM, Bonner J, Maricq AV, Benian GM, Norman KR (2012). Large isoforms of UNC-89 (obscurin) are required for muscle cell architecture and optimal calcium release in Caenorhabditis elegans. PLoS One 7, e40182.

Thompson O, Edgley M, Strasbourger P, Flibotte S, Ewing B, Adair R, Au V, Chaudhry I, Fernando L, Hutter H, *et al*. (2013). The million mutation project: a new approach to genetics in Caenorhabditis elegans. Genome Res 23, 1749–1762.

Warner A, Xiong G, Qadota H, Rogalski T, Vogl AW, Moerman DG, Benian GM (2013). CPNA-1, a copine domain protein, is located at integrin adhesion sites, and is required for myofilament stability in Caenorhabditis elegans. Mol Biol Cell 24, 601–616.

Waterhouse A, Bertoni M, Bienert S, Studer G, Tauriello G, Gumienny R, Heer FT, de Beer TAP, Rempfer C, Bordoli L, *et al*. (2018). SWISS-MODEL: homology modelling of protein structures and complexes. Nucleic Acids Res 46, W296–W303.

Wilson KJ, Qadota H, Benian GM (2012). Immunofluorescent localization of proteins in Caenorhabditis elegans muscle. Methods Mol Biol 798, 171–181.

Zaidel-Bar R, Joyce MJ, Lynch AM, Witte K, Audhya A, Hardin J (2010). The F-BAR domain of SRGP-1 facilitates cell-cell adhesion during C. elegans morphogenesis. J Cell Biol 191, 761–769.

Supplementary Materials
Molecular Biology of the Cell
Martin *et al*.

Supplemental Figure 1

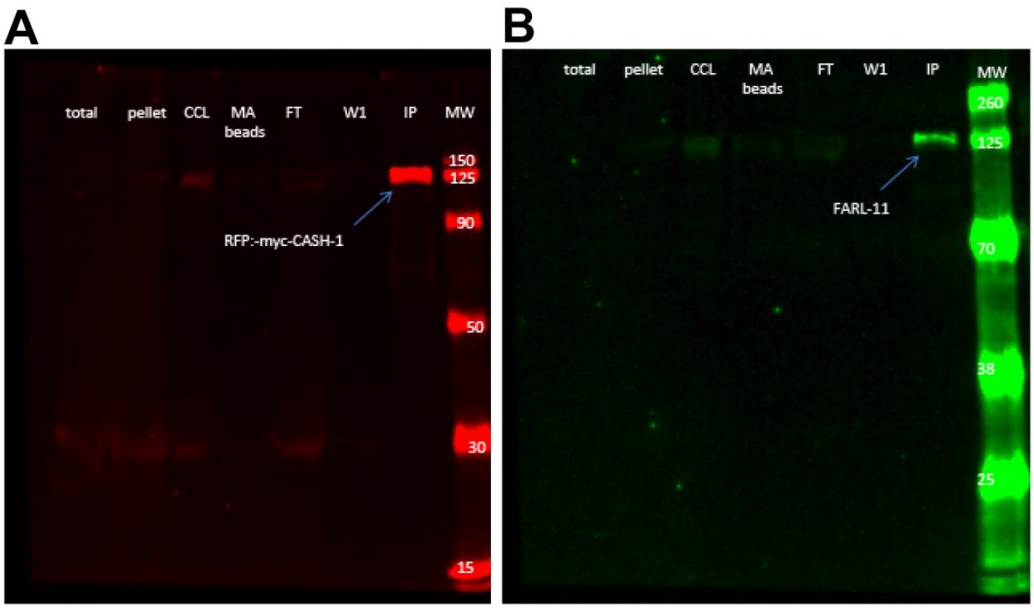

Supplemental Figure 1. Co-immunoprecipitation of FARL-11 with CASH-1, with detailed controls. As described in Materials and Methods, TagRFP-myc-CASH-1 was immunoprecipitated from a lysate of strain SU854, and proteins from consecutive steps of the procedure were separated by SDS-PAGE, blotted and incubated with anti-myc (A) or with anti-FARL-11 (B). From left to right the lanes of each blot contain: (1) total lysate (total), (2) insoluble proteins pelleted from total lysate (pellet), (3) clarified cell lysate (CCL), (4) proteins associated with magnetic agarose control beads (MA beads), (5) proteins that did not bind to anti-RFP magnetic agarose or flow-through (FT), (6) proteins in first wash of anti-RFP magnetic agarose (W1), (7) proteins eluted from anti-RFP magnetic agarose (IP), and (8) molecular weight markers (MW) with sizes indicated in kDa. Arrows indicate the positions of RFP-myc-CASH-1 or FARL-11 in the IP. In (A) note that RFP-myc-CASH-1 is detectable in the worm lysate (CCL lane) and was immunoprecipitated (IP lane). In (B) note that FARL-11 was detectable in the worm lysate (CCL lane) and was co-immunoprecipitated (IP lane).

Supplemental Figure 2

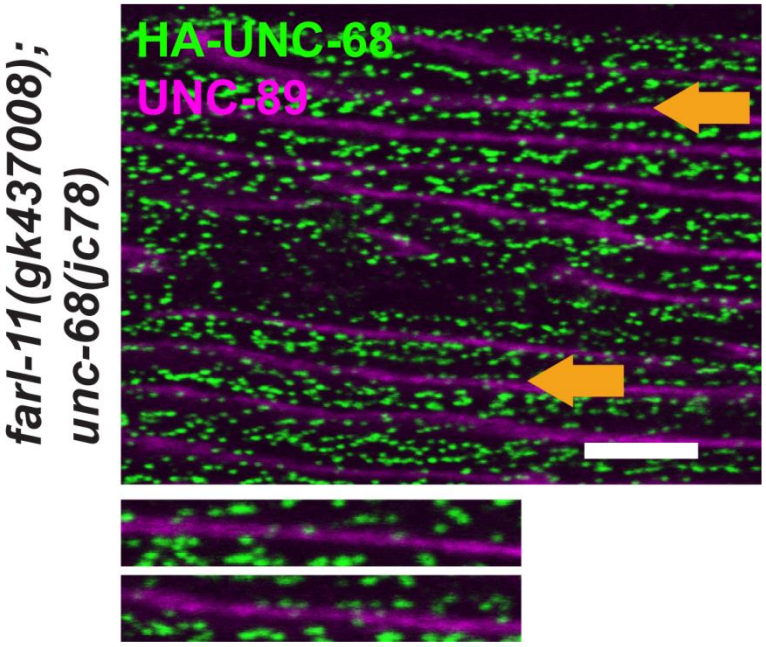

Supplemental Figure 2. Imaging of GB352 which expresses HA-UNC-68 in a *farl-11(gk437008)* mutant background, immunostained with anti-HA and anti-UNC-89, an alternative way to mark M-lines (shown in magenta). Note that in the zoomed-in images that there are fewer HA-UNC-68 small puncta surrounding M-lines, as compared to wild type shown in Figure 9A. Scale bar, 10 μm.

Supplementary Table 1. Penetrance of body wall muscle sarcomeric defects in mutants.

For each of the mutant alleles listed, the organization of each sarcomeric component was observed in 10 animals. The percentages represent the fraction of 10 animals showing the phenotype. Note that the penetrance varies from 70 to 100%, even among various alleles of the same gene (e.g. *cash-1*).

Supplementary Table 1

gene	allele	Disorganization of		
		UNC-95	UNC-89	MHC A
cash-1	*gk705529*	70%	90%	70%
cash-1	*jc100*	70%	80%	90%
cash-1	*syb4646*	100%	100%	100%
farl-11	*jc93*	100%	100%	100%
farl-11	*jc94*	100%	100%	100%
farl-11	*gk437008*	100%	100%	100%
unc-68	*e540*	70%	100%	90%